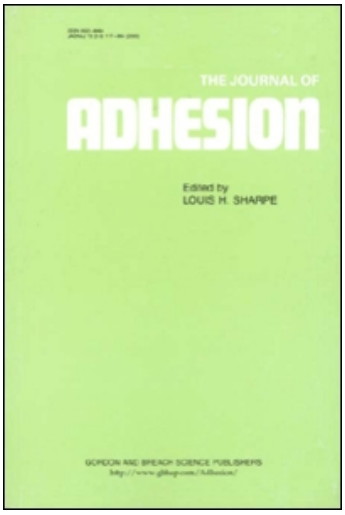

The Journal of Adhesion

Publication details, including instructions for authors and subscription information:
http://www.informaworld.com/smpp/title~content=t713453635

A Simple Constant Strain Energy Release Rate Loading Method for Double Cantilever Beam Specimens

David A. Dillard[a]; John Z. Wang[a]; Hari Parvatareddy[a]
[a] Department of Engineering Science and Mechanics, Virginia Polytechnic Institute and State University, Blacksburg, Virginia, U.S.A.

To cite this Article Dillard, David A. , Wang, John Z. and Parvatareddy, Hari(1993) 'A Simple Constant Strain Energy Release Rate Loading Method for Double Cantilever Beam Specimens', The Journal of Adhesion, 41: 1, 35 — 50
To link to this Article: DOI: 10.1080/00218469308026553
URL: http://dx.doi.org/10.1080/00218469308026553

J. Adhesion, 1993, Vol. 41, pp. 35–50
Reprints available directly from the publisher
Photocopying permitted by license only

Printed in the United States of America.

A Simple Constant Strain Energy Release Rate Loading Method for Double Cantilever Beam Specimens*

DAVID A. DILLARD, JOHN Z. WANG and HARI PARVATAREDDY

Department of Engineering Science and Mechanics, Virginia Polytechnic Institute and State University, Blacksburg, Virginia 24061, U.S.A.

(Received July 29, 1991; in final form May 21, 1992)

A simple loading arrangement is proposed to permit nearly constant strain energy release rate testing of double cantilever beam specimens. The inexpensive arrangement may be well suited to long term and environmental exposure testing of these specimens. An added advantage of the technique is that it also provides an attractive method to measure debond length. The geometrically nonlinear loading device provides constant strain energy release rate loading under idealized conditions. Analysis of the technique for realistic conditions reveals the appropriate test window for the device, and allows design guidelines to be developed. Experimental evaluation confirms the analytical predictions.

KEY WORDS double cantilever beam specimen; constant strain energy release rate test method; environmental exposure testing; fracture test method; adhesive fracture; durability.

INTRODUCTION

The fracture toughness is an important parameter in characterizing the strength of adhesive joints. The (flat) double cantilever beam (DCB) specimen, as depicted in Figure 1, is commonly used for measuring G_{IC}, the critical strain energy release rate. The first application of the DCB specimen in experimental mechanics was made by Obreimoff in 1930 in testing the crack propagation of monolithic materials.[1] In the 1960s, the DCB specimen configuration was introduced into the adhesive industry by Ripling and Mostovoy to test the Mode I fracture energy of adhesively bonded joints.[2–4] Modifications in the geometry and loading arrangement permit fracture testing with various mixtures of Mode I, II, and III.[5–10] Later, the DCB specimen was adopted to study the delamination behavior of composite materials.[11–13] Corrections for adhesive thickness have also been introduced.[14–16] The approximate strain energy release rate of the DCB specimens as given by Ripling and Mostovoy[2–4] is:

*Presented at the Fifteenth Annual Meeting of The Adhesion Society, Inc., Hilton Head Island, South Carolina, U.S.A., February 17–19, 1992. One of a Collection of papers honoring A. J. Kinloch, the recipient in February 1992 of *The Adhesion Society Award for Excellence in Adhesion Science, Sponsored by 3M*.

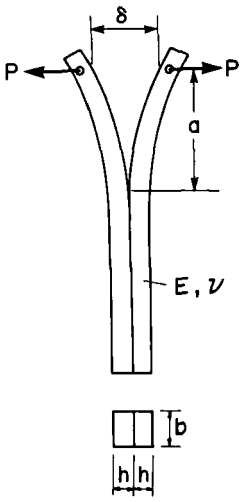

FIGURE 1 A symmetrically loaded double cantilever beam specimen with relevant dimensions.

$$G_I = \frac{4P^2}{Eb^2}\left[\frac{3a^2}{h^3} + \frac{1}{h}\right] \tag{1}$$

where

P = the force acting perpendicular to the bondline
a = crack length
h = the thickness of the adherend
b = the width of the adherend and bondline
E = the Young's modulus of the adherend

The first term in the brackets is due to bending, while the second term is a correction for shear.

For sufficiently long debonds, Equation (1) indicates that the strain energy release rate of the specimen subjected to a constant load is almost proportional to the square of the crack length. Since the strain energy release rate increases rapidly with crack length, specimens would tend to fail catastrophically under constant load conditions, so constant displacement rate conditions are normally used for experimental purposes. The Boeing wedge test [ASTM D3762] has been widely used and advocated as a sensitive durability test for adhesives[17] and is simply a DCB specimen loaded under constant displacement conditions. For this loading mode, the strain energy release rate decreases as the inverse of the fourth power of the crack length. Regardless of the loading mode, the DCB specimen exhibits a strong dependence of the strain energy release rate on the debond length. Generally speaking, special effort is needed to prevent unstable crack growth and special instrumentation is required to obtain an accurate measurement of the crack length.

is constant lengthwise. Although such a specimen produces a constant strain energy release rate under constant load conditions, the manufacturing difficulty is much higher than that for the flat DCB specimen.

This paper will introduce a new experimental method which is intended to produce a nearly constant strain energy release rate with the flat DCB specimen configuration. Besides this advantage, the scheme may also simplify the instrumentation for measuring the crack length growth. It is expected that this inexpensive loading mode could be quite appropriate for long-term or durability testing, although one should be cautioned about the interpretation of environmental exposure data for DCB specimens where diffusion from the sides may progressively weaken the specimen.[14]

TEST GEOMETRY ANALYSIS

The proposed experimental setup is depicted in Figure 2. The major feature of the experimental setup is that the loading is accomplished with a cable attached to the specimen. A constant load is applied at the mid-point of the span between points A and B by means of a dead weight. It is well known that a linear elastic cable loaded in this manner produces a deflection proportional to the cube root of the applied load. This property offsets the functional dependence of Equation (1) on crack length to result in a constant strain energy release rate, as is now shown.

Applying classical mechanics theories to the setup in Figure 2, one may obtain the following basic relations:

Equilibrium

$$W = 2P\sin\theta \tag{2}$$

Kinematics

$$\frac{L}{\cos\theta} - L = \delta + \Delta L_c \tag{3}$$

$$\Delta = \frac{L}{2}\tan\theta \tag{4}$$

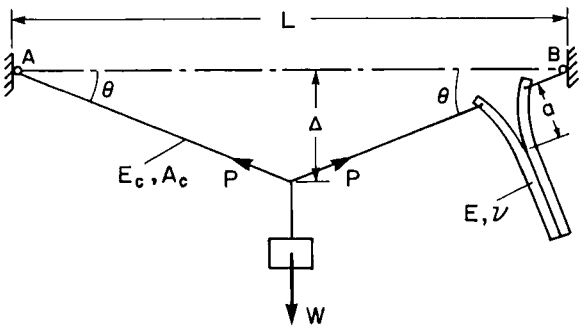

FIGURE 2 The proposed loading fixture with relevant dimensions and parameters.

Energy Balance

$$G_I = \frac{4P^2}{Eb^2}\left[\frac{3a^2}{h^3} + \frac{1}{h}\right] \tag{5}$$

Constitutive

$$\delta = \frac{8Pa^3}{Ebh^3} \tag{6}$$

$$\Delta L_c = \frac{PL_c}{E_c A_c} \tag{7}$$

where the parameters (as illustrated in Figure 2) are:

W = the applied load
L = the distance between points A and B
δ = the crack opening displacement
Δ = the vertical displacement of load W
L_c = the total length of the cable
E_c = the Young's modulus of the cable
A_c = the cross-sectional area of the cable
θ = the angle of the cable measured from horizontal

For correctness, the properties of the cable should be adjusted to include the flexibility of the supports.

As a first approximation, if the assumptions are made that the angle θ is small $\left(\sin\theta \approx \theta, \cos\theta \approx 1 - \frac{\theta^2}{2}\right)$, the cable is inextensible $\left(\frac{E_c A_c}{L_c} \approx \infty\right)$, and the shear effect in the strain energy release rate is negligible $\left(G_I \approx \frac{12P^2a^2}{Eb^2h^3}\right)$, the following expressions can be derived from Equations (2)–(7):

$$G_I' = \frac{3WL}{4bh}\left(\frac{W}{EbL}\right)^{1/3} \tag{8}$$

and

$$a = \frac{h}{L}\left(\frac{W}{EbL}\right)^{-1/3}\Delta' \tag{9}$$

The prime on G_I and Δ indicates that these quantities are obtained under the above mentioned assumptions. Limitations will be pointed out in subsequent figures.

From Equation (8), it is apparent that under the assumptions of small θ, inextensible cable, and negligible shear effect, the strain energy release rate does not depend on the crack length, a, and, therefore, is constant as the crack grows. Interestingly, the dependence of the DCB strain energy release rate on crack length is offset by the geometrically nonlinear nature of a loaded cable, resulting in a constant strain energy release rate test method. An added advantage is apparent from Equa-

tion (9). It is seen that one may be able to obtain the crack length by measuring the load displacement, Δ, with a linear variable differential transducer (LVDT) or other device. This is especially useful since detecting the location of a debond front is not simple, especially during environmental exposure.

If the exact effect of angle θ, the deformation of the cable, and the shear effect are considered, the following expressions can be obtained from Equations (2)–(7):

$$\bar{G}_I = \left[\frac{2}{\dfrac{(1+\cos\theta)\cos\theta}{\bar{a}^3 + \dfrac{\bar{k}}{8}}}\right]^{2/3} \left[\frac{1}{3} + \bar{a}^2\right] \tag{10}$$

$$\bar{\Delta} = \frac{\tan\theta}{2\bar{W}^{1/3}\bar{a}} \tag{11}$$

where θ is determined by

$$\frac{(1-\cos\theta)\sin\theta}{\cos\theta} = 4\bar{W}\left(\bar{a}^3 + \frac{\bar{k}}{8}\right) \tag{12}$$

and the various nondimensional parameters in Equations (10), (11), and (12) are defined as:

$$\bar{G}_I = \frac{G_I}{G_I'} \tag{13}$$

$$\bar{\Delta} = \frac{\Delta}{\Delta'} \tag{14}$$

$$\bar{a} = \frac{a}{h} \tag{15}$$

$$\bar{W} = \frac{W}{EbL} \tag{16}$$

$$\bar{k} = \frac{EbL_c}{E_cA_c} \tag{17}$$

It is important to grasp the physical significance of each of these terms. $\bar{G}_I$ is the ratio of the more exact value for the strain energy release rate to the value obtained from Equation 8 with the simplifying assumptions. Similarly $\bar{\Delta}$ represents the analogous relationship for load displacement. It is convenient to express them in this manner because nondimensionalized plots can later be presented indicating the accuracy of the simple equations (8 and 9) which, remarkably, indicated that G_I is independent of crack length, and Δ is proportional to crack length. The other nondimensional terms are also convenient. $\bar{W}$ represents a normalized load term, and $\bar{k}$ represents the specimen stiffness normalized with respect to the cable stiffness. (In the calculation for the strain energy release rate, Equations (2) and (3) and the Taylor series expansion for $\cos\theta$ indicate that the cable tension is inversely proportional to the square root of the DCB opening displacement. This leads to the elimination of thickness cubed in the $\bar{k}$ term.)

From Equations (10) to (12), one may see that, for a given $\bar{a}$, $\overline{G}_I$ and $\bar{\Delta}$ are determined by $\bar{k}$ and $\overline{W}$. The parameter $\bar{k}$ indicates the degree of the relative deformation of the cable to that of the DCB specimen. When $\bar{k}$ is zero, the cable is rigid or inextensible. As $\bar{k}$ increases, the assumption of inextensibility of the cable becomes less applicable. From Equations (6) and (7), it can be shown that the ratio of the deformation of the DCB specimen to that of the cable is proportional to a^3. Therefore, we would expect that as the crack length increases, the influence of $\bar{k}$ on $\overline{G}_I$ and $\bar{\Delta}$ becomes less significant. However, at very short crack lengths, the influence of $\bar{k}$ on $\overline{G}_I$ and $\bar{\Delta}$ is pronounced.

The effect of the normalized load, $\overline{W}$, on $\overline{G}_I$ and $\bar{\Delta}$ is through its effect on the angle θ. At small crack length, θ can be expected to be small. However, as the crack length increases, θ will become larger. Theoretical and numerical analysis indicate that, at relatively long crack lengths $\left(\bar{a} > \left(\frac{\bar{k}}{2}\right)^{1/3}\right)$, θ can be considered to be dependent only on $\overline{W}$. θ is a monotonically increasing function of $\overline{W}$. Therefore, as $\overline{W}$ increases, the small angle assumption becomes less applicable. In short, the above discussions indicate that the normalized specimen stiffness, $\bar{k}$, influences $\overline{G}_I$ and $\bar{\Delta}$ at shorter crack lengths while the normalized load, $\overline{W}$, influences $\overline{G}_I$ and $\bar{\Delta}$ at longer crack lengths. Increases in $\bar{k}$ and $\overline{W}$ will cause deviations of $\overline{G}_I$ and $\bar{\Delta}$ from unity in their respective regions of influence.

At crack initiation, when $\overline{G}_I$ is near unity, $\overline{W}_c$ can be approximated from Equation (8) as:

$$\overline{W}_c = \left(\frac{4G_{Ic}h}{3EL^2}\right)^{3/4} \tag{18}$$

The c subscripts on $\overline{W}$ and G_I denote the critical values causing debonding.

Before discussing plots showing the influence of $\bar{k}$ and $\overline{W}$ on $\overline{G}_I$ and $\bar{\Delta}$, we suggest a typical geometry so that we can identify a realistic range of operation. By assuming h as the minimum adherend thickness at which yielding in the adherends does not occur, and $L = 1.0$ meter, the ranges of $\overline{W}$ for different adherend-adhesive systems are estimated. These values are indicated in Table I. In the calculations, the fracture toughness values are taken from Reference 18. The value of $\bar{k}$ depends on the

TABLE I
Typical values of $\overline{W}_c$ and $\bar{k}$

Adherend	Adhesive	$\overline{W}_c$	$\bar{k}^c$
Steel	Unmodified Epoxy ($G_{IC} = 58 \sim 177\ J/m^2$)[a]	$2.67 \times 10^{-10} \sim 1.42 \times 10^{-9}$	325~1310
	Rubber Toughened Epoxy ($G_{IC} = 700 \sim 3900\ J/m^2$)[b]	$1.12 \times 10^{-8} \sim 1.47 \times 10^{-7}$	
Aluminum	Unmodified Epoxy ($G_{IC} = 58 \sim 177\ J/m^2$)[a]	$1.08 \times 10^{-9} \sim 5.77 \times 10^{-9}$	108~442
	Rubber Toughened Epoxy ($G_{IC} = 700 \sim 3900\ J/m^2$)[b]	$4.53 \times 10^{-8} \sim 5.97 \times 10^{-7}$	

[a]Data from Table I in Ref. 18
[b]Data from Fig. 10 in Ref. 18
[c]$\bar{k}$ was based on $L_c = 1.0$ m, $d_c = 3.2$ mm~6.4 mm

selection of the cable material as well as its size. If graphite fibers are used as the cable material, and the cable diameter is chosen between 3.2 mm to 6.4 mm and the cable length L_c as 1.0 meter ($L_c \approx L$), the obtained ranges of $\bar{k}$ for different adherends are shown in Table I.

Attempts to solve Equations (10) to (12) in a closed form would encounter complicated, high-order algebraic equations. Therefore, numerical approaches were used to evaluate the behavior.

Figures 3 to 6 are the numerical results of the effects of $\bar{k}$ and $\bar{W}$ on the behavior of $\bar{G}_I$ and $\bar{\Delta}$. In these figures, the ranges of $\bar{W}_c$ and $\bar{k}$ in Table I are also indicated.

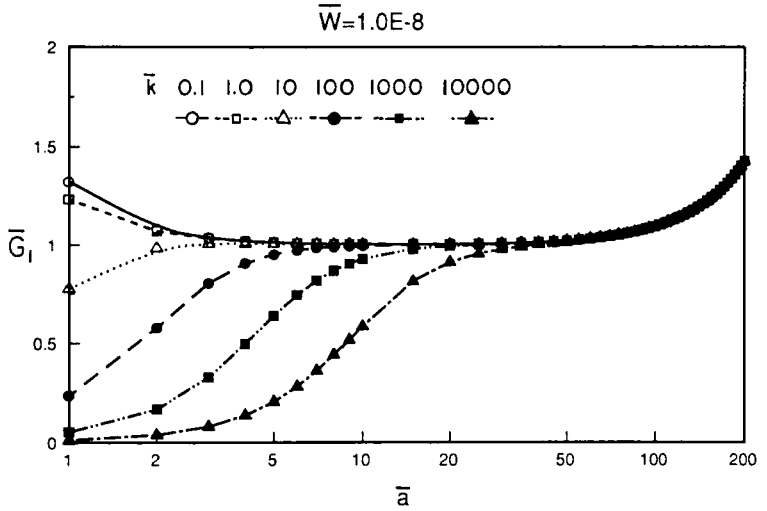

FIGURE 3 The normalized strain energy release rate as a function of normalized crack length for several specimen stiffness parameters.

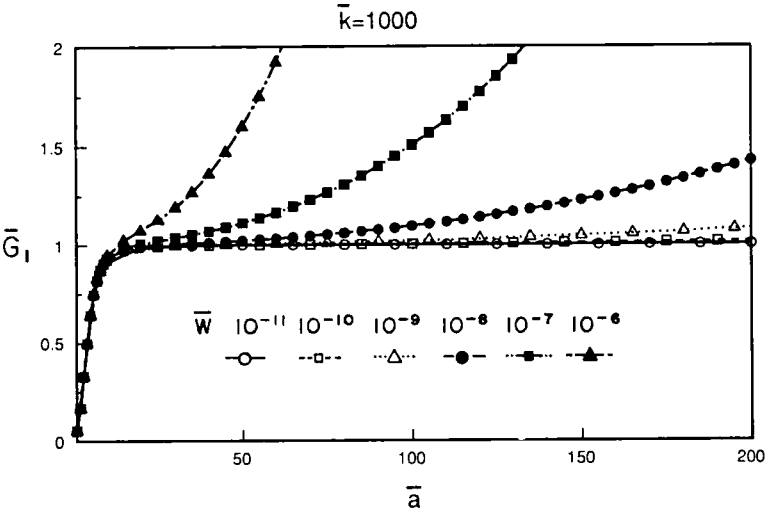

FIGURE 4 The normalized strain energy release rate as a function of normalized crack length for several normalized load values.

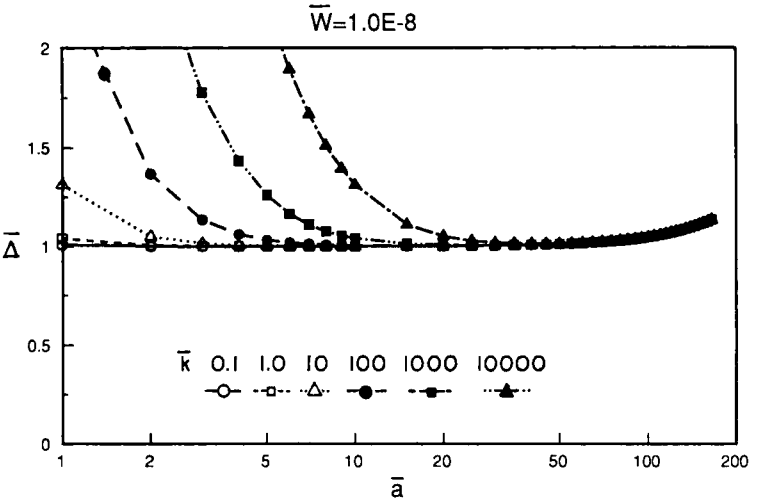

FIGURE 5 Normalized load deflection as a function of normalized crack length for several specimen stiffness parameters.

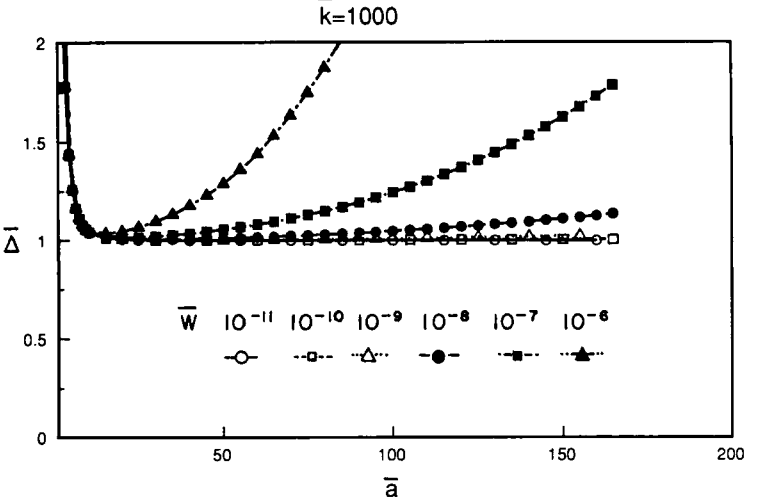

FIGURE 6 Normalized load deflection as a function of normalized crack length for several normalized load values.

Figures 3 and 5 show the influence of $\bar{k}$ on the behavior of $\bar{G}_I$ and $\bar{\Delta}$, respectively. Figures 4 and 6 show the influence of $\bar{W}$ on the behavior of $\bar{G}_I$ and $\bar{\Delta}$. For the purpose of clarity, a logarithmic scale on the horizontal axis has been used in Figures 3 and 5 to show the behavior of $\bar{G}_I$ and $\bar{\Delta}$ at shorter crack lengths. These results verify the above analysis. For example, in Figure 3, the values of $\bar{G}_I$ at different $\bar{k}$ differ only at shorter crack lengths. At longer crack lengths, $\bar{G}_I$ converges to the same value for a given crack length. Even though not shown here, at sufficiently long crack lengths $\left(\bar{a} > \left(\frac{\bar{k}}{2}\right)^{1/3}\right)$, both $\bar{G}_I$ and $\bar{\Delta}$ are increasing functions of θ. When θ

is less than 20°, $\overline{G}_I$ and $\bar{\Delta}$ are between 1.00 and 1.05. Violating the small angle assumption thus introduces only small errors.

EXPERIMENTAL VALIDATION

In order to assess the accuracy of the proposed loading device, a loading frame was constructed for testing DCB specimens. A large beam was used to support the specimen and the opposite end of a 3 mm steel cable. Since it is critical that the cable be just taut before a load is applied, a turnbuckle was included in the load train to adjust the cable tension correctly prior to testing. Adherend pairs were clamped at various distances to simulate different debond lengths. Loads of varying magnitude were applied by hanging weights midway between the supports on the suspended cable. Load deflection, Δ, and DCB opening displacement, δ, were measured at each load and debond length. The strain energy release rate was calculated from the geometry and Equations (2), (4), and (5). Similar results were also obtained by using the opening displacements, δ.

Several specimens were used for the experimental evaluation. In all cases, excellent agreement was obtained for Equation (9) and the experimentally observed load displacement. A typical result is shown in Figure 7. In most cases, the strain energy release rate, as shown in Figure 8, was relatively independent of the debond length, although there was a slight deviation between the G predicted by Equation (8) and that obtained from the experiment, as indicated in the preceding paragraph. More recent tests on actual bonded samples have shown that the agreement with Equation (8) is considerably better.

We are currently fabricating a multi-station test frame which will suspend five DCB specimens above water in a heated water bath. Occasional load cycling will

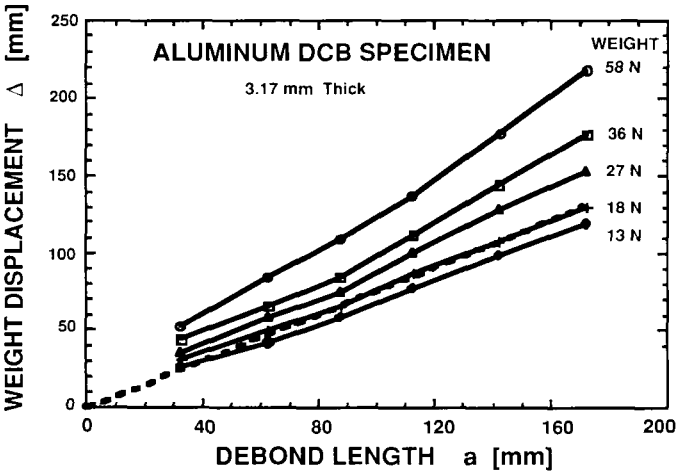

FIGURE 7 Load displacement, Δ, *versus* debonded length, a, for aluminum adherends and several applied loads. The prediction from Eqn. 9 is shown for the case of an applied load of 18 N.

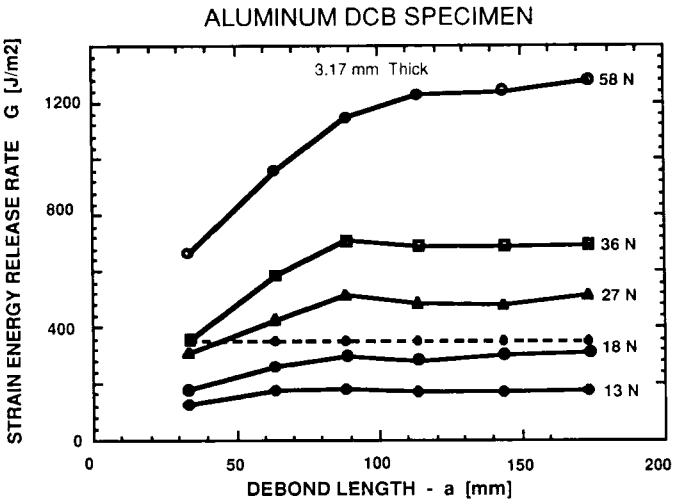

FIGURE 8 Strain energy release rate, G_I, *versus* debond length, a, for aluminum adherends and several applied loads. The prediction from Eqn. 8 is shown for the case of an applied load of 18 N.

be achieved by the use of a pair of air cylinders which will raise and lower the weights. Results from these constant strain energy release rate tests may be reported in future publications.

DESIGN CONSIDERATIONS

In implementing this loading method for the DCB specimen, stable time-dependent crack propagation and simplified data acquisition and reduction can be obtained if $\overline{G}_I$ and $\bar{\Delta}$ remain equal to unity, so that G_I and Δ/a are constant as the crack grows. However, as shown above, due to the influence of deformation of the cable and the effect of larger angles, $\overline{G}_I$ and $\bar{\Delta}$ may deviate from unity at shorter and longer crack lengths. Therefore, a criterion is needed to define a region within which $\overline{G}_I$ and $\bar{\Delta}$ closely approximate unity. Equivalently, we seek the range of crack length $\bar{a}_0 \leq \bar{a} \leq \bar{a}_1$, which satisfies:

$$| \overline{G}_I - 1 | \leq \alpha \quad \text{when } \bar{a}_0^{(G_I)} \leq \bar{a} \leq \bar{a}_1^{(G_I)} \tag{19}$$

and

$$| \bar{\Delta} - 1 | \leq \alpha \quad \text{when } \bar{a}_0^{(\Delta)} \leq \bar{a} \leq \bar{a}_1^{(\Delta)} \tag{20}$$

where α is the acceptable amount of error.

From the above discussions, one may see that $\bar{a}_0$ is mainly dependent on $\overline{k}$ and $\bar{a}_1$ on $\overline{W}$. Obviously, both $\bar{a}_0$ and $\bar{a}_1$ are functions of α. Numerical analysis of Equations (10), (11), (12), (19), and (20) allows one to obtain the following approximate results:

$$\bar{a}_1^{(G_I)} = 0.59 \frac{\alpha^{0.407}}{\bar{W}^{1/3}} \tag{21}$$

$$\bar{a}_0^{(\Delta)} = 0.306 \frac{\bar{k}^{1/3}}{\alpha^{0.355}} \tag{22}$$

$$\bar{a}_1^{(\Delta)} = 0.913 \frac{\alpha^{0.493}}{\bar{W}^{1/3}} \tag{23}$$

The dependence of $\bar{a}_0^{(G_I)}$ on $\bar{k}$ and α is less obvious. To determine the dependence for a particular set of values of $\bar{k}$ and α, one may need to consult a plot such as shown in Figure 9 or perform a numerical analysis using Equations (10), (12), and (19).

In designing the test setup, one may need to consider, among others, the following factors: the prevention of yielding in the adherends, the selection of design parameters to ensure a satisfactory range between a_0 and a_1, the load to be applied (at least an estimate), and the limitation in available space.

To prevent yielding in the adherends, the following criterion must be met:

$$h \geq h_{\min} = \frac{3EG_{IC}}{\sigma_y^2} \tag{24}$$

When α is small (say 0.05), the load to cause crack growth may be estimated as:

$$W_c = b\left(\frac{64\,(G_{IC}h)^3E}{27L^2}\right)^{1/4} \tag{25}$$

At a certain value of α, a_0 and a_1 can be selected according to the following criteria:

$$a_0 = \max\{h\bar{a}_0^{(\Delta)},\ h\bar{a}_0^{(G_I)},\ a_0^{(\sigma)}\} \tag{26}$$

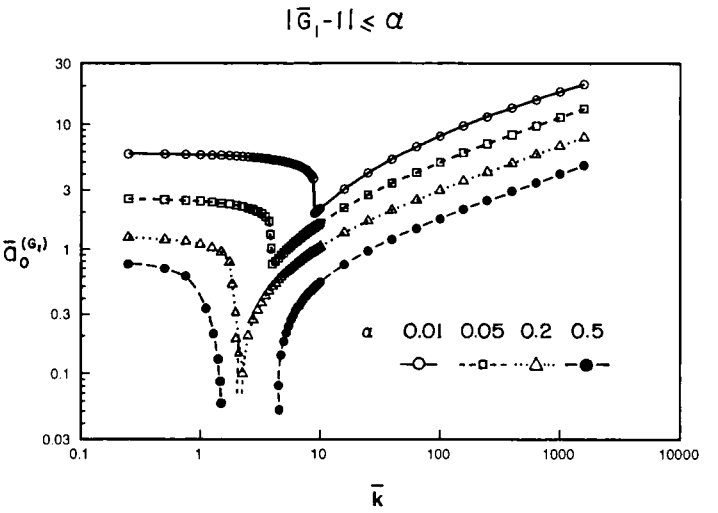

FIGURE 9 Design criterion for the minimum initial debond length for several acceptable errors.

$$a_1 = \min\{h\bar{a}_1^{(\Delta)}, h\bar{a}_1^{(G_I)}\} \tag{27}$$

where $a_0^{(e)}$ is the crack length at which the end effect can be considered negligible (e.g., $a_0^{(e)} = 3h$).

To increase the useful crack length range, one may wish to maximize the ratio a_1/a_0. However, it would not be feasible or necessary to choose too large a value for the ration because of the end effect and space limitation. To reduce the end effect, a_0 should be sufficiently greater than the adherend thickness (e.g., $a_0/h > 3$). To save space, the total length of the specimen should not be excessively greater than a_1. Using the above design guidelines, some numerical examples are obtained as reported in Table II.

AN ALTERNATIVE FORM OF SETUP

In the setup shown in Figure 2, the specimen weight may introduce problems in certain configurations, including the possibility of mixed mode behavior. If it is necessary to keep the specimen vertical, the setup shown in Figure 10 may be adopted. The changes of $\overline{G}_I$ and $\bar{\Delta}$ with respect to $\bar{a}$ at various $\overline{k}$ and $\overline{W}$ values are shown in Figures 11–14. Because a given value of DCB opening displacement, δ, effectively shortens the distance between the suspended cable supports rather than

TABLE II
Design examples ($\alpha = 0.05$)

	Unmodified epoxy ($G_{IC} = 120\ J/m^2$)	Rubber-toughened epoxy ($G_{IC} = 2300\ J/m^2$)
	Specimen Geometry: $h = 1.59$ mm ($h_{min} = 0.94$ mm) $b = 25.4$ mm 16 mm $\leq a \leq$ 262 mm	Specimen Geometry: $h = 25.4$ mm ($h_{min} = 18.0$ mm) $b = 25.4$ mm 149 mm $\leq a \leq$ 1000 mm
Steel Adherend $E = 204\ GPA$ $\sigma_y = 280\ MPA$	Cable* Geometry: $d_c = 6.4$ mm, $L_c = 1000$ mm Critical Load: $W_c = 6.1$ N Crack Length Measurement: $a = 1.504\Delta$	Cable* Geometry: $d_c = 12.7$ mm, $L_c = 1000$ mm Critical Load: $W_c = 447.6$ N Crack Length Measurement: $a = 5.746\Delta$
	Specimen Geometry: $h = 3.17$ mm ($h_{min} = 2.05$ mm) $b = 25.4$ mm 21 mm $\leq a \leq$ 335 mm	Specimen Geometry: $h = 45$ mm ($h_{min} = 39.3$ mm) $b = 25.4$ mm 178 mm $\leq a \leq$ 1171 mm
Aluminum Adherend $E = 69\ GPA$ $\sigma_y = 110\ MPA$	Cable* Geometry: $d_c = 6.4$ mm, $L_c = 1000$ mm Critical Load: $W_c = 7.8$ N Crack Length Measurement: $a = 1.927\Delta$	Cable* Geometry: $d_c = 12.7$ mm, $L_c = 1000$ mm Critical Load: $W_c = 524.2$ N Crack Length Measurement: $a = 6.729\Delta$

*Cable Material: Graphite Fibers ($E = 250\ GPA$)

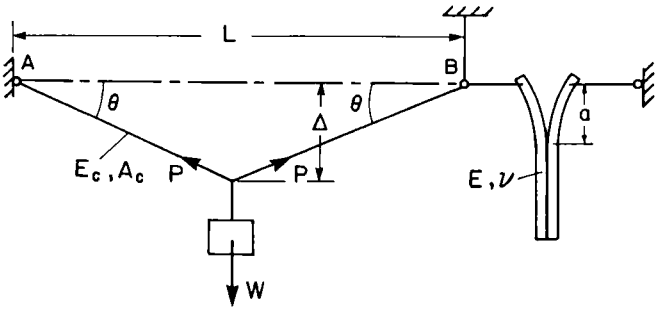

FIGURE 10 An alternative loading device for DCB specimens which allows the specimen to hang vertically.

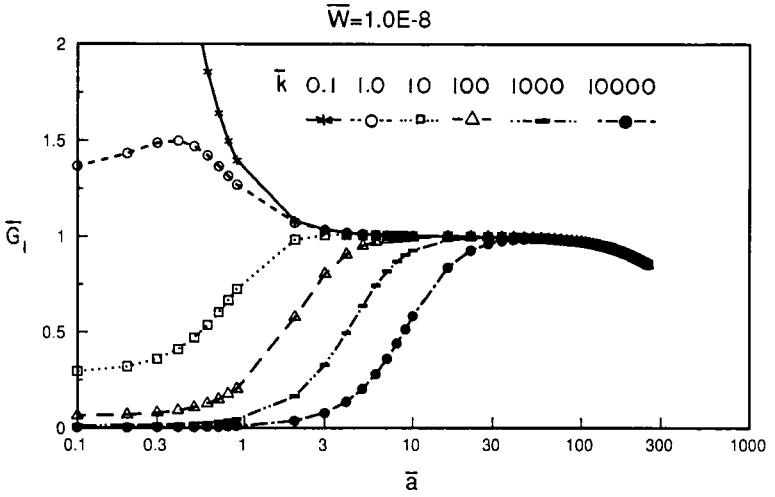

FIGURE 11 The normalized strain energy release rate as a function of normalized crack length for several specimen stiffness parameters for alternate loading device.

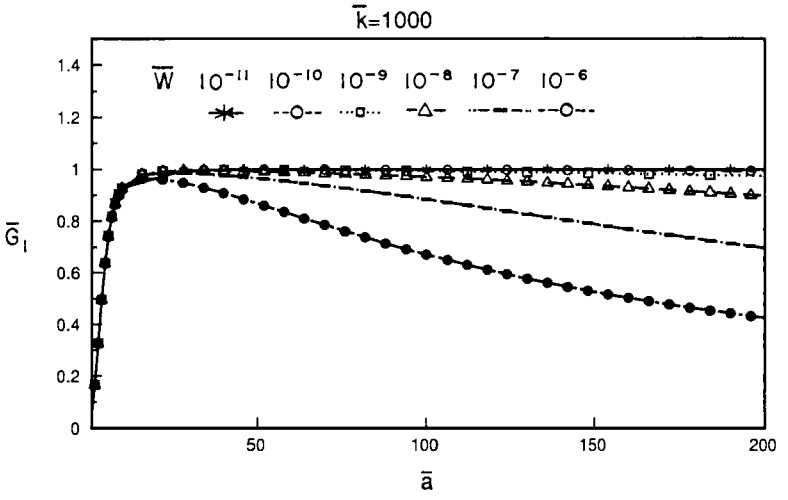

FIGURE 12 The normalized strain energy release rate as a function of normalized crack length for several normalized load values for alternate loading device.

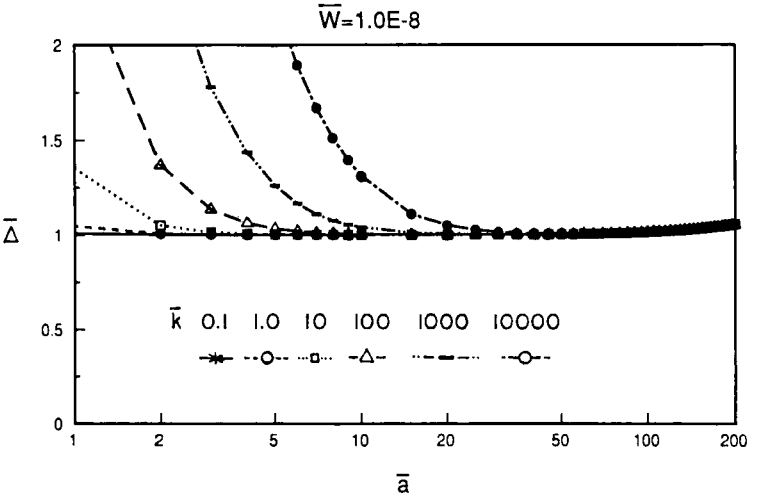

FIGURE 13 Normalized load deflection as a function of normalized crack length for several specimen stiffness parameters for alternate loading device.

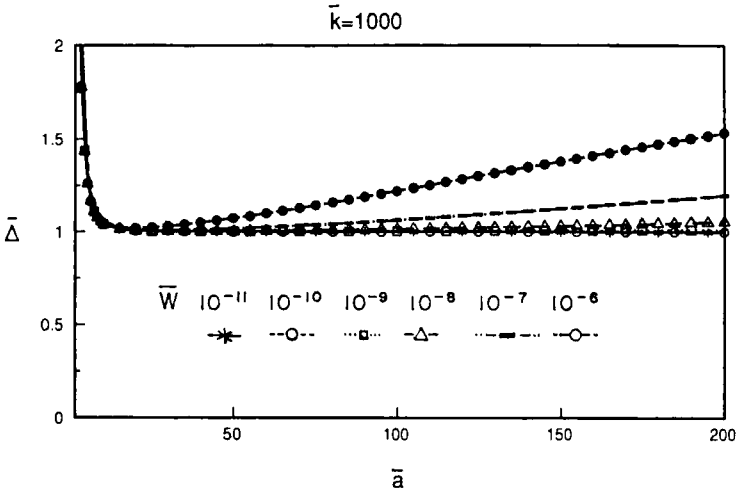

FIGURE 14 Normalized load deflection as a function of normalized crack length for several normalized load values for alternate loading device.

lengthening the cable (as with the prior configuration), distinctly different equations are obtained. With the similar procedures to those for the setup in Figure 1, the following results can be obtained

$$\tilde{a}_1^{(G_I)} = 2.72 \frac{\alpha^{0.823}}{\overline{W}^{1/3}} \tag{28}$$

$$\tilde{a}_0^{(\Delta)} = 0.294 \frac{\overline{k}^{1/3}}{\alpha^{0.386}} \tag{29}$$

$$\bar{a}_1^{(\Delta)} = 3.04 \frac{\alpha^{0.726}}{\overline{W}^{1/3}} \tag{30}$$

The exact expressions for $\bar{a}_0^{(G_I)}$ depend on α and $\bar{k}$. They are graphically shown in Figure 15.

For the alternate configuration (denoted with primes), one may find that $a_0' \approx a_0$ and $a_1' \approx 1.32 a_1$. Even though this setup configuration results in a longer usable range of crack length and more pure Mode I crack extension, it requires a supporting cable or pulley at point B, thus complicating the design. Nonetheless, it is an attractive design for certain situations.

SUMMARY AND CONCLUSIONS

A simple loading scheme is proposed for fracture tests on flat DCB specimens. The device consists of a light, taut cable with one end fastened to a rigid support and the other end fastened to one leg of the DCB specimen. The second leg of the DCB pivots about a rigid support, and a dead weight is applied at the midpoint of the cable. Under idealized conditions, the geometrically nonlinear loading device produces a strain energy release rate which is independent of debond extension. This inexpensive loading configuration can be used to simplify testing and data analysis for simple DCB specimens, especially for long term or environmental exposure studies. Another significant ramification of this constant strain energy release rate characteristic is that a dead weight will move through a distance which is proportional to the debond extension. Conceptually, this could eliminate the need for special or time-consuming techniques to monitor debond propagation. The simple loading method thus eliminates several problems associated with the flat DCB specimen: 1) unstable debond growth because of increasing G_I under constant load

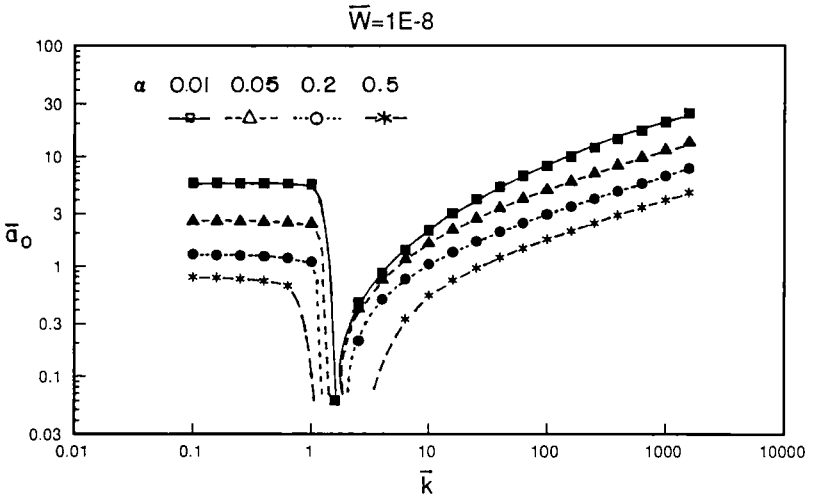

FIGURE 15 Design criterion for the minimum initial debond length for several acceptable errors for alternate loading device.

conditions, 2) accurate means to detect debond length, and 3) data reduction necessary to calculate the strain energy release rate as a function of crack length.

Under realistic conditions, cable extension reduces the accuracy of the technique for short crack lengths, and large angles of cable rotation may reduce accuracy for cases where the cable is short, the weight is heavy, and crack extension is large. Nonetheless, for typical material systems and reasonable geometries, fairly wide test windows can be achieved within which the constant strain energy release rate and weight displacement proportional to debond length characteristics are quite accurate. The paper provides some guidelines to design appropriate geometries for implementing the test.

The desirable features of this loading method, and minimal costs, may make long term or environmental exposure testing of DCB specimens more practical. Experimental implementation of this technique is currently underway.

Acknowledgements

This material is based upon work supported by the National Science Foundation under Grant No. DMR-8809714. The Government has certain rights in this material. The authors are also grateful to the Dow Company for providing the impetus to develop this practical loading method.

References

1. J. W. Obreimoff, *Proc. Roy. Soc. Lond.* **A127,** 290–297 (1930).
2. E. J. Ripling, S. Mostovoy, and R. L. Patrick, *Mat. Res. Stand.* MTRSA, ASTM, **64(3),** 129–134 (1964).
3. S. Mostovoy, P. B. Crosley, and E. J. Ripling, *J. Mater.* **2,** 661–681 (1967).
4. E. J. Ripling, H. T. Corten, and S. Mostovoy, *J. Adhesion,* **3,** 107–123 (1971).
5. P. D. Mangalgiri, W. S. Johnson, and R. A. Everett, Jr., *J. Adhesion* **23,** 263–288 (1987).
6. H. Chai, *International J. Fracture* **37,** 137–159 (1988).
7. E. J. Ripling, P. B. Crosley, and W. S. Johnson, "A Comparison of Pure Mode I and Mixed-Mode I-II Cracking of an Adhesive Containing an Open Knit Cloth Carrier," in *Adhesively Bonded Joints: Testing, Analysis, and Design,* W. S. Johnson, Ed., **STP 981** (American Society for Testing and Materials, Philadelphia, 1988), p. 163–182.
8. P. W. Osborne, *Rev. Sci. Instrum.* **37,** 664 (1966).
9. A. J. Russell and K. N. Street, "Factors Affecting the Interlaminar Fracture Energy of Graphite/Epoxy Laminates", in *Progress in the Science and Engineering of Composites,* T. Hayashi, K. Kawata, and S. Unekawa, Eds. (Pergamon Publishing, New York, 1982), p. 279–286.
10. A. J. Russell and K. N. Street, "Moisture and Temperature Effects on the Mixed Mode Delamination Fracture of Unidirectional Graphite/Epoxy", in *Delamination and Debonding of Materials,* W. S. Johnson, Ed., **STP 876** (American Society for Testing and Materials, Philadelphia, 1985), p. 349–370.
11. P. Yeung and L. J. Broutman, *Polym. Eng. Sci.* **18,** 62–67 (1978).
12. J. M. Whitney, C. E. Browing, and W. Hoogsteden, *J. Reinf. Plast. Comp.* **1,** 297–313 (1982).
13. D. F. Devitt, R. A. Schapery and W. L. Bradly, *J. Comp. Mater.* **14,** 270–285 (1980).
14. D. R. Lefebvre, D. A. Dillard and H. F. Brinson, *Experimental Mechanics* **28,** 38–44 (1988).
15. M. B. Ouezdou, A. Chudnovsky and A. Moet, *J. Adhesion* **25,** 169–183 (1988).
16. D. L. Hunston, A. J. Kinloch and S. S. Wang, *J. Adhesion* **28,** 103–114 (1989).
17. J. A. Filbey and J. P. Wightman, *J. Adhesion* **28,** 1–22 (1989).
18. D. B. Willard, *et al., J. Appl. Polym. Sci.: Appl. Polym. Symposia* **32,** 165–188 (1977).